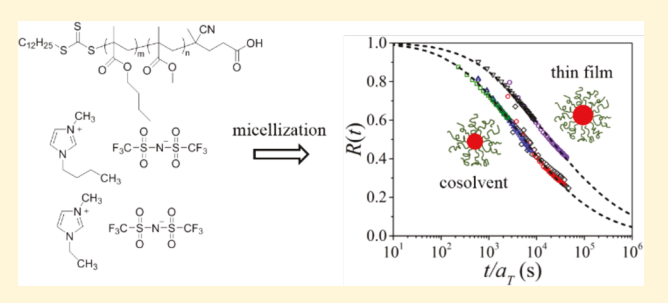
Exchange Kinetics for a Single Block Copolymer in Micelles of Two **Different Sizes**

Dan Zhao, Yuanchi Ma, and Timothy P. Lodge*, to be a longe to be a longer and Timothy P. Lodge

†Department of Chemistry and ‡Department of Chemical Engineering and Materials Science, University of Minnesota, Minneapolis, Minnesota 55455, United States

Supporting Information

ABSTRACT: The effect of micellar size on the chain exchange kinetics in spherical micelles consisting of poly(methyl methacrylate)-block-poly(n-butyl methacrylate) (PMMA-b-PnBMA) in a mixture of ionic liquids (1-ethyl-3-methylimidazolium bis(trifluoromethylsulfonyl)imide, [EMIM][TFSI], and 1-butyl-3-methylimidazolium bis(trifluoromethylsulfonyl)imide, [BMIM][TFSI]) was investigated using time-resolved small-angle neutron scattering (TR-SANS). Two spherical micelles with different core sizes were prepared from a single block copolymer by using different protocols. In one case the



micelles were formed in the presence of a cosolvent, while in the other a polymer thin film was directly dissolved in the ionic liquid. Interestingly, the micelle core size prepared from the latter method is ~30% larger than that obtained in the former case. TR-SANS experiments reveal that the rate of single chain exchange in the micelles with a larger core size is slowed down by ~3 times compared to the smaller core radius. This can be possibly attributed to the smaller interfacial area per chain, and larger corona density, for micelles with a larger core dimension. These geometrical factors can potentially lead to changes in both the attempt time and activation barrier for chain expulsion during the unimer exchange process. Our results clearly suggest that, in addition to the molecular characteristics of the block copolymer and solvent, the geometrical structure of the micelle plays an important role in the unimer dynamic exchange processes in block copolymer micelles.

INTRODUCTION

The self-assembly of block copolymers (BCPs) into various micellar nanostructures in a selective solvent or polymeric melt is of widespread fundamental interest and may enable a host of diverse applications including drug and gene delivery, 1-3 cell membrane stabilization,⁴ tissue engineering,⁵ viscosity modification, design of nanoreactors, and toughening of plastics. 8-10 To fully realize these practical uses, it is desirable to understand the molecular-level mechanisms responsible for BCP micellization and equilibration. Abundant evidence suggests that unimer exchange among discrete micelles plays a vital role in establishing these nanoscale structures, especially when the system is close to its thermodynamically stable state. 11 Various approaches have been used to study micellization kinetics, including temperature-jump light scattering, 12 ultracentrifugation, 13 fluorescence spectroscopy, 14,15 and transmission electron microscopy. 16,17 In the past decade, a novel time-resolved small-angle neutron scattering (TR-SANS) technique has been developed and used to reveal the critical molecular characteristics, including core block chain length $(N_{\rm core})$, dispersity, core block/solvent interaction parameter, corona chain length (N_{corona}), and chain architecture, that can affect the kinetics of molecular exchange processes. 18-25 For instance, Choi et al. 19 have reported that the molecular exchange is hypersensitive to N_{core} , and also observed a linear dependence of the activation barrier on N_{core} , rather than the

scaling with ${N_{\rm core}}^{2/3}$ proposed by Halperin and Alexander. This linear dependence of energy barrier on $N_{\rm core}$ was also confirmed in other systems. Although this discrepancy between experiments and theory can be reconciled by the possible scenario that the expelled insoluble block remains partially swollen rather than being fully collapsed, 19,28 other factors could also play a role. For example, the curvature of the micelle core/corona interface as well as the corona density profile should vary with $N_{\rm core}$, which could possibly affect the molecular exchange process. ^{27,29} To this end, Lund et al. reported slightly accelerated kinetics for spherical micelles compared to their cylindrical counterparts, which was attributed to subtle changes in the corona structure.²⁷ As a result, a comprehensive understanding of micelle formation and equilibration should take all these factors into account. Examination of the structural effects in spherical micelles (e.g., micelle core size, corona density) is the primary focus of this report.

To realize structural control over micelle formation for fixed molecular characteristics of block copolymer and solvent at the same experimental conditions (e.g., temperature), here we build on the seminal work by Eisenberg's group, 30-32 later extended

Received: December 1, 2017 Revised: February 17, 2018 Published: March 13, 2018



Table 1. Molecular Characteristics of PMMA-b-PnBMA Diblock Copolymers^a

polymer	$M_{\rm n,PMMA}^{b}$ (kg/mol)	$M_{\rm n,PnBMA}^{b}$ (kg/mol)	$N_{ m PMMA}^{^c}$	$N_{ m PnBMA}^{c}$	\mathcal{D}^d
PMMA- <i>b</i> -PnBMA (25–53)	25	53	250	373	1.08
PMMA- <i>b</i> - <i>d</i> PnBMA (25–54)	25	54	250	358	1.09

^aAs reported in ref 24. ${}^bM_{n,PMMA}$ and $M_{n,PnBMA}$ are number-averaged molecular weights of the PMMA and PnBMA blocks, respectively. ${}^cN_{PMMA}$ and N_{PnBMA} are the degrees of polymerization of the two blocks. dD ispersity of the diblock copolymer.

by Meli and Lodge, who have shown that distinct yet narrow distributions of spherical micelles can be obtained depending on the preparation procedure.^{33,34} Although this strongly suggests the complicated role of nonergodic states in dispersions of block copolymers, it also provides a means to examine the effect of micellar geometrical structure on the micelle relaxation processes (decoupled from the chain characteristics, with the same micelle morphology) and particularly the kinetics of chain exchange. We conducted TR-SANS experiments to investigate the role of micellar size on the chain exchange kinetics in spherical diblock copolymer micelles in ionic liquids (ILs). Two sets of micelles were prepared by different protocols but using identical block copolymer chains, poly(methyl methacrylate)-block-poly(nbutyl methacrylate) (PMMA-b-PnBMA), in a mixture of ionic liquids (30 wt % 1-butyl-3-methylimidazolium bis(trifluoromethylsulfonyl)imide), [BMIM][TFSI] and 70 wt % 1-ethyl-3methylimidazolium bis(trifluoromethylsulfonyl)imide, [EMIM][TFSI], denoted as "30% [BMIM]" in the following text). As shown in the previous studies, ^{24,35-37} PnBMA displays a lower critical solution temperature (LCST) in both ionic liquids and forms the micelle cores, while PMMA is always soluble in these two solvents and is the corona-forming block. This implies that PnBMA is more soluble at lower temperatures. Consequently, thermal annealing at higher temperatures may not accelerate the chain exchange kinetics. The temperature-dependent monomeric friction and thermodynamic incompatibility vary in opposite directions with temperature in an LCST system.²⁴ Additionally, the solvent selectivity for the PnBMA block can be tuned by varying the ratio of the two homologous solvents in the mixture. 35,37 Here 30% [BMIM] was used as the solvent in order to bring the time scale of chain exchange into the time window of a typical TR-SANS experiment.24 Small-angle X-ray scattering (SAXS) and dynamic light scattering (DLS) confirmed significant differences in the micelle core size and corona density between these two sets of micelles. Interestingly, TR-SANS reveals that these structural differences lead to distinct rates of chain exchange: significantly slower for micelles possessing a larger core.

EXPERIMENTAL SECTION

Synthesis and Characterization. A nearly identical pair of PMMA-b-PnBMA diblock copolymers (one with "normal" PnBMA and the other with partially deuterated PnBMA, or dPnBMA, using d_9 -n-butyl methacrylate as the monomer) was synthesized by sequential radical addition—fragmentation chain-transfer (RAFT) polymerization, as described previously. The number-average molecular weight (M_n) and dispersity (D) for both diblocks were characterized using a combination of size exclusion chromatography (SEC) with a multiangle laser light scattering detector (Wyatt DAWN) and ¹H nuclear magnetic resonance spectroscopy (¹H NMR, Varian Inova 500). The detailed procedures can be found in a previous report, ²⁴ and the characterization results are shown in Table 1. Note that most of the structural characterization was performed based on the hydrogenated diblock copolymer, unless otherwise specified. However, some

structural information for equivalent micelles formed with deuterated chains is provided in Table S1 of the Supporting Information.

The ionic liquids [EMIM][TFSI] and [BMIM][TFSI] were prepared by ion exchange reactions.³⁸ Partially deuterated versions were synthesized by isotopic exchange of the three hydrogens on the imidazole ring, based on an established method.³⁹ Note that in some cases the three hydrogens were not completely isotopically exchanged, but the net degree of deuteration, determined by ¹H NMR spectroscopy, is sufficient to make the contrast-matching solvent mixture. Additionally, ¹H NMR characterization of the ionic liquids was conducted in deuterated dimethyl sulfoxide (*d*₆-DMSO), with a 10 s decay to ensure full relaxation of the imidazole hydrogens. The ¹H NMR spectra of the ionic liquids are presented in Figure S1. All other chemicals were purchased from Sigma-Aldrich and used as received.

Sample Preparation. Two distinct protocols were used to prepare micellar solutions in ionic liquids. Unless otherwise specified, the polymer concentration was 1 wt %. In the cosolvent method (CS), a copolymer and ionic liquid mixture in a predetermined ratio was dissolved in a good solvent, dichloromethane (DCM). The resulting solution was then purged with filtered nitrogen overnight to slowly remove the cosolvent until constant weight was achieved and further dried at 50 °C under vacuum (<100 mTorr) for 12 h. Complete removal of DCM in the final solutions was confirmed by ¹H NMR. In the thin film (TF) protocol, copolymer was first deposited on the walls of the glass vial by casting from DCM. Afterward, the appropriate amount of ionic liquid mixture was added, and the copolymer was directly dissolved at 80 °C for at least 2 h. Note that ¹H NMR experiments performed on solutions of copolymer and ionic liquid in deuterated acetone show that complete polymer dissolution can be achieved after only 2 h (Figure S2), presumably due to the low polymer concentration and the low glass transition temperature (T_g) of the solvophobic PnBMA block ($T_g \approx 20$ °C).⁴⁰ Note that direct dissolution (DD) of the bulk polymer could also be used to prepare micellar solutions.³³ Here the TF protocol is preferred because it is practically much easier to dissolve all the polymer into the ionic liquid, and thus ensure the exact polymer concentration in the final solution, due to the fluffy nature of the dry polymer, combined with the high viscosity and low vapor pressure of the ionic liquid. In the current work, the micellar solutions prepared by both CS and TF procedures were then annealed at 55 °C for 2 h prior to measurements, unless otherwise noted.

Dynamic Light Scattering (DLS). DLS experiments were performed on a Brookhaven BI-200SM multiangle light scattering instrument with a 637 nm laser or on a DynaPro NanoStar at a fixed scattering angle of 90° with a laser wavelength of 663 nm. All measurements were conducted at 55 °C unless otherwise noted. The micelle solutions (1 wt % copolymer) were passed through 0.45 μ m filters to remove dust and then flame-sealed under vacuum in a glass tube to avoid contact with moisture in air and prevent polymer degradation. In a typical thermal relaxation experiment, the normalized intensity autocorrelation function, $g^{(2)}(t)$, was measured at a 90° scattering angle and varying time intervals. The acquisition time for each measurement was 5-10 min. Additionally, in the middle of each thermal relaxation experiment, $g^{(2)}(t)$ was also collected at several scattering angles ranging from 30° to 110°. The measured $g^{(2)}(t)$ was well-represented by a second-order cumulant fit, from which an average decay rate $(\overline{\Gamma})$ and the normalized second cumulant $(\mu_2/\overline{\Gamma}^2)$, or dispersity) can be obtained.⁴¹ The mutual diffusion coefficient (D_m) was calculated as $D_{\rm m} = \overline{\Gamma}/q^2$, assuming dilute solution conditions; here *q* is the scattering wavevector, defined as $q = (4\pi n/\lambda) \sin(\theta/2)$, *n* is the refractive index of the solvent, λ is the vacuum laser wavelength, and θ

is the scattering angle. For analysis of data collected over a range of scattering angles, $D_{\rm m}$ was extracted from a linear fit of $\bar{\Gamma}$ vs q^2 , with imposed zero intercept. The apparent hydrodynamic radius $(R_{\rm h})$ was then calculated according to the Stokes–Einstein relation, $R_{\rm h}=k_{\rm B}T/(6\pi\eta D_{\rm m})$, where $k_{\rm B}$ is Boltzmann constant, T is the absolute temperature, and η is the solvent viscosity. The correlation functions were also analyzed by the REPES Laplace inversion algorithm to obtain the size distributions.

Small-Angle X-ray Scattering (SAXS). SAXS experiments were carried out on the 5-ID-D beamline of the Dupont–Northwestern–Dow Collaborative Access Team (DND-CAT) at the Advanced Photon Source, Argonne National Laboratory, operating at a wavelength of 0.73 Å and a sample-to-detector distance of 8.50 m. This provides a q range of $\sim 0.0024-0.13$ Å $^{-1}$. In typical runs, the micelle solutions were transferred into 1.5 mm quartz capillaries and sealed with parafilm. 2-D scattering data were collected at 55 °C using a Rayonix CCD area detector, typically with a 1 s beam exposure, and then averaged azimuthally to provide 1-D scattering intensity I(q) vs q profiles. Subsequently, the background-corrected intensity traces were analyzed based on the Pedersen model for block copolymer micelles combined with the Percus–Yevick structure factor, as described elsewhere. 36,43,44

Time-Resolved Small-Angle Neutron Scattering (TR-SANS). TR-SANS experiments were performed to characterize the chain exchange kinetics among diblock copolymer micelles. Briefly, two populations of equivalent micelles, either CS or TF (one with protonated and the other with deuterated core blocks), were prepared in a contrast-matching solvent mixture (with the same scattering length density as the average of the protonated and deuterated cores, i.e., $\rho_{\text{sol}} = (\rho_{\text{PnBMA}} + \rho_{d\text{PnBMA}})/2$, Table S2). After mixing equal masses of the two micelle solutions, the rate of chain exchange was measured from the decrease in the scattering intensity upon redistribution of the core block chains. Specifically, at time t = 0, the scattering intensity I(q,0) is at its maximum. As time elapses, the protonated/deuterated (h-/d-) chains are randomly expelled and then inserted into different micelles, leading to a decrease in the core scattering length density difference and thus lower scattering intensity I(q,t). Finally, at $t=\infty$, all micelles will be on average consist of equal amounts of h- and dchains; hence, the coherent scattering intensity $I(q,\infty)$ of the micelle cores is essentially zero. To quantify the extent of chain exchange, a normalized relaxation function is defined, 22 as given by

$$R(t) = \sqrt{\frac{I(q, t) - I(q, \infty)}{I(q, 0) - I(q, \infty)}}$$
(1)

Clearly, at t = 0, R(t) = 1 while at $t = \infty$, R(t) = 0. I(q,t) was directly measured from the scattering of the postmixed solutions (mixtures of equal amount of h- and d-micelles), I(q,0) was taken as the average of the scattering intensities of the separate h- and d-micelle solutions, and $I(q,\infty)$ was determined from scattering of a premixed sample, which was prepared by blending a 50/50 mixture of the h- and d-block copolymers before micelles were formed; thus, the resulting micelle cores on average possess equal number of h- and d-chains.

The TR-SANS experiments were performed on the NG7 30m SANS beamline at the Center for Neutron Research of the National Institute of Standards and Technology (NIST).⁴⁵ Data were collected using an instrument configuration with a wavelength of 6.0 Å, a wavelength spread $(\Delta \lambda/\lambda)$ of 0.22, and a sample-to-detector distance of 4.7 m, providing a q range of $\sim 0.007 - 0.1 \text{ Å}^{-1}$. As noted earlier, to provide the same sample history, all the separate h- and d-micelle solutions prepared by both protocols were annealed at 55 °C for 2 h prior to the TR-SANS experiments. In a typical time-resolved run, equal masses of h- and d-micelle solutions were first thermally equilibrated at a specified temperature (25, 35, or 55 °C) and thoroughly mixed to prepare the postmixed solution. The postmixed sample was then quickly transferred into a 1 mm thickness demountable titanium cell and then placed on the beamline for data acquisition. Note that although the temperature change of the micelle solutions was abrupt at some point of the experiments (e.g., from 55 to 25 °C), this should not affect the TR-SANS results, as the micellar

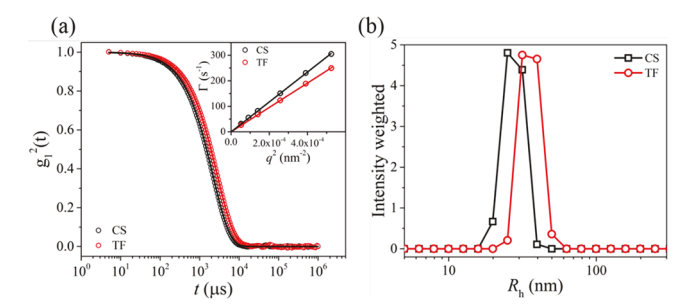


Figure 1. (a) Normalized squared electric field correlation functions $g_1^2(t)$ vs decay time t for 1 wt % micelle solutions in 30% [BMIM] ionic liquid at T=55 °C and scattering angle $\theta=90$ °. The black and red symbols correspond to the CS and TF micelles, respectively; the solid lines are the cumulant fits. The inset shows the linear fits to the decay rate vs q^2 for both micellar systems. (b) Representative hydrodynamic radius distributions for CS (black) and TF (red) micelles obtained from REPES analysis at $\theta=90$ °.

structure does not evolve significantly with temperature and time under these experimental conditions (see Figure S3). The scattering pattern was continuously recorded for 5 min intervals, for a total duration of 2–3 h. The isotropic 2-D scattering patterns were then reduced and converted to 1-D data using the Igor Pro package developed by NIST. More details about the TR-SANS experiments and data analyses can be found in a previous report. 24

■ RESULTS AND DISCUSSION

Figure 1a presents the representative normalized squared electric field correlation functions, $g_1^2(t)$, as a function of decay time at 55 °C for micelles prepared from both CS and TF procedures. Evidently, $g_1^2(t)$ for the TF micelles decays at a later time than the CS ones, indicating a larger size for micelles obtained from the TF method. The correlation functions were first analyzed by REPES to obtain the hydrodynamic radius (R_h) distributions, from which a single, narrowly distributed population was observed for both micelles (Figure 1b). Therefore, $g_1^2(t)$ can be modeled by the cumulant expansion, and a linear relationship between $\overline{\Gamma}$ vs q^2 was verified (inset of Figure 1a). This analysis gives an average R_h of 33.5 and 28.0 nm as well as $\mu_2/\overline{\Gamma}^2$ of 0.04 and 0.03 for the TF and CS micelles, respectively, which is consistent with the size distributions in Figure 1b. At least three more solutions were prepared and measured for both methodologies, and similar results were obtained. Collectively, these data show that both procedures can yield well-defined micelles with narrow size distributions, but with a distinctly larger R_h value observed for the TF micelles. These DLS results are qualitatively consistent with the finding from Meli and Lodge,³³ who also observed a larger steady-state hydrodynamic size of polybutadiene-b-poly-(ethylene oxide) (PB-b-PEO) micelles in [EMIM][TFSI] prepared by the TF protocol than that obtained from the CS method.

To probe the effect of solution processing on the micelle core dimensions, SAXS measurements were conducted on both CS and TF samples. As shown in Figure 2, in either case, the scattering intensity oscillates at higher values of q and levels off in the low q regime. These scattering features suggest formation of well-defined spherical micelles, with no larger structure or aggregation in the solutions. As the scattering is dominated by the core (the ratio of the squared total excess scattering lengths of the corona and the core block $\beta_{\rm corona}^2/\beta_{\rm core}^2$ is ~ 0.09), ³⁶ the position of the first q minimum (q_1) can be directly related to the micelle core size. As can be seen in Figure 2, q_1 in the TF

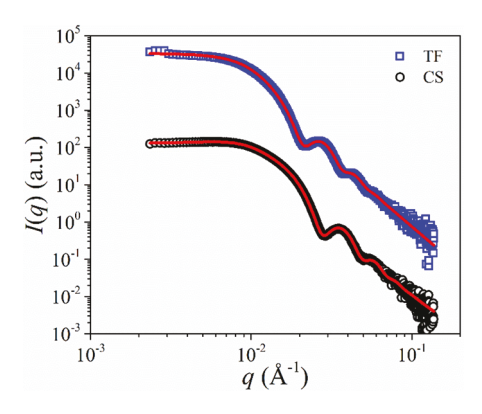


Figure 2. SAXS intensity I(q) vs scattering wavevector q for 1 wt % CS (black circles) and TF (blue squares) micelles in 30% [BMIM] ionic liquid at 55 °C. The red solid lines represent best fits to the Pedersen model with the Percus–Yevick structure factor. ³⁶ Note that the profile for the TF sample was vertically shifted by a factor of 100 for clarity.

sample appears at a lower q value than in the CS case, indicating that the micelle core size is larger for micelles prepared by the former protocol (also confirmed by the SANS measurements, Figure S3b). The scattering profiles for both micellar solutions can be well described by the Pedersen model with a hard sphere structure factor (the solid red lines in Figure 2, with the primary fitting parameters presented in Table 2 and the remainder in Table S3), from which $R_c = 15.3$ and 19.7 nm were obtained for the CS and TF micelles, respectively. These fitting results agree well with the estimated values ($R_c = 15.5$ and 19.5 nm for the CS and TF micelles) from the characteristic equation for the minima in the spherical form factor, $tan(qR_c)$ $-qR_c=0$, with $qR_c=4.49$ at the first minimum. In other words, the micelles prepared via the TF protocol have a core radius ~30% larger than that obtained from the CS method, consistent with the DLS results. Three separate samples were prepared by the TF method, all of which yield roughly the same SAXS profile and core size (Figure S4).

On the basis of the SAXS analysis, the corona thickness can be estimated as the difference between $R_{\rm h}$ and $R_{\rm c}$. As shown in Table 2, the corona thickness is slightly larger for the TF micelles (the corona thickness was also estimated from the difference between the hard sphere radius $R_{\rm hs}$ and $R_{\rm c}$ which is ~ 15 nm for both micelles, Table S3). Therefore, the difference in the overall micelle size originates primarily from the distinct core dimensions. This can be reconciled by the fact that the micelles were formed in different solvent environments. In the CS case, the micelles were initially formed in the process of cosolvent evaporation, i.e., when the core block/solvent interaction becomes slightly worse than theta conditions. The micelles are expected to grow as cosolvent evaporation continues, and ultimately the morphology will be locked in when nearly all of the unimers are consumed. In other words,

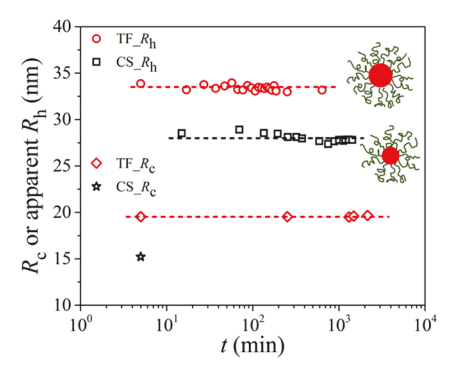


Figure 3. Micelle core radius (R_c) or the apparent hydrodynamic size (R_h) vs time for 1 wt % CS (black symbols) and TF (blue symbols) micelles in 30% [BMIM] ionic liquid at 55 °C. The dashed lines are drawn as guides to the eye. The cartoons indicate different core dimensions of micelles prepared by the CS or TF method. Note that all measurements started after the micelle solutions had already been annealed at 55 °C for 2 h. Additionally, the micellar solution for the R_h measurements is a mixture of equal amount of h- and d-micelles, while that for the R_c measurements consists of only h-micelles.

the core dimension of the CS micelles reflects an equilibrium state in the presence of a certain amount of cosolvent, which should be smaller than the equilibrium size in the pure ionic liquid. Indirect evidence for this argument lies in the fact that the micellar hydrodynamic size distribution and core dimension are insensitive to the composition of the ionic liquid mixtures ([BMIM]% = 0-30%) or the core block/ionic liquid interaction ($\chi_{PnBMA/IL}$), as long as the micelles were prepared via the CS protocol (Figure S5). In contrast, in the TF method the micelles were directly formed in the ionic liquid solvent, where the interaction between PnBMA and the ionic liquid is already significantly unfavorable to drive micelle formation. 24,37 It is therefore the difference in $\chi_{PnBMA/solvent}$ when the micelles were first formed that leads to the distinct core sizes in these two micellar solutions. In fact, TF micelles prepared at a higher temperature (or larger $\chi_{PnBMA/IL}$, e.g., 150 °C, due to the LCST behavior) indeed have an even larger hydrodynamic size (Figure S6), supporting this interpretation. This finding also reflects the fact that the TF micelles tend to increase the aggregation number $(N_{\rm agg})$ so as to reduce the interfacial area per chain $(a_0$ in Table 2) and thus reduce the interfacial free energy between the core block and the corona/IL mixture. These results agree well with the observations from Meli and Lodge in a micellar system consisting of PB-b-PEO in [EMIM][TFSI].

We examined the stability of the micellar structure in both systems as a function of time using DLS and SAXS, where the micelle solutions were annealed at 55 $^{\circ}\mathrm{C}$ for varying amounts of time. As shown in Figure 3, R_{c} and R_{h} for both CS and TF micelles are nearly constant with time, at least within a 10 h

Table 2. Physical Characteristics of 1 wt % Diblock Copolymer Micelles in 30 wt % [BMIM] Ionic Liquid

	$R_{\rm h}^{a}$ (nm)	$\mu_2/\overline{\Gamma}^{2a}$	$R_{\rm c}^{a}$ (nm)	σ_{R}^{a} (nm)	$N_{ m agg}^{b}$	s_{PnBMA}^{c}	$a_0^d (nm^2)$	L_{corona}^{e} (nm)	s_{PMMA}^{f}	$\rho_{\rm corona}^{\rm g}$ (monomers/nm ³)
CS	28.0	0.03	15.3	1.4	180 ± 50	1.3 ± 0.1	161 ± 1.5	12.7	1.3 ± 0.2	0.6 ± 0.1
TF	33.5	0.04	19.7	2.2	390 ± 130	1.7 ± 0.2	12.5 ± 1.4	13.8	1.4 ± 0.2	0.8 ± 0.2

^aTime-averaged value of the data in Figure 3, where $\sigma_{\rm R}$ is the standard deviation of the $R_{\rm c}$ distribution. $^bN_{\rm agg}$ is calculated as $4\pi R_{\rm c}^{\ 3}/(3\nu_{\rm PnBMA})$, assuming that the core is devoid of solvent, where $\nu_{\rm PnBMA}$ is the volume per core chain. $^cs_{\rm PnBMA}$ is the degree of core block stretching, i.e., $R_{\rm c}$ divided by the mean square end-to-end distance of the core block. da_0 is the interfacial area per chain, calculated as $4\pi R_{\rm c}^{\ 2}/N_{\rm agg}$. $^cL_{\rm corona}$ is the corona thickness, estimated as $R_{\rm h} - R_{\rm c}$. $^fs_{\rm PMMA}$ is the degree of corona block stretching, i.e., $L_{\rm corona}$ divided by the mean square end-to-end distance of the corona block. $^g\rho_{\rm corona}$ is the average monomer density in the corona region, calculated as $3N_{\rm agg}N_{\rm PMMA}/(4\pi(R_{\rm h}^{\ 3} - R_{\rm c}^{\ 3}))$.

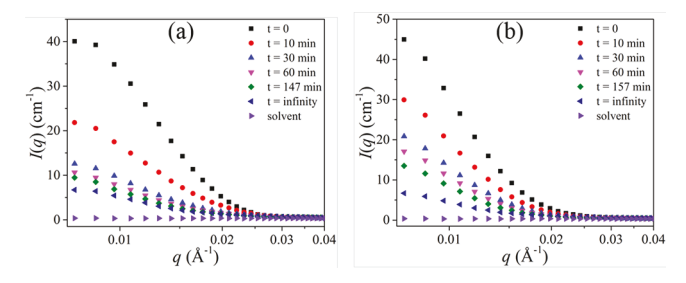


Figure 4. Representative TR-SANS profiles I(q) vs q for 1 wt % postmixed (a) CS and (b) TF micellar solutions in 30% [BMIM] at 55 °C and varying times, as indicated inside the plot. Note that "t = infinity" corresponds to the scattering of the premixed sample.

time window (also confirmed by the SANS measurements, Figure S3b). Moreover, prolonged thermal annealing experiments up to 2 weeks still show essentially no change in micelle hydrodynamic size (Figure S6). Clearly, via different preparation protocols, two steady-state size distributions of micelles were obtained from the identical block copolymer in the same ionic liquid solvent. Similar results were also reported by Meli and Lodge.³³

Now we consider the effect of micelle size on the molecular exchange kinetics. Representative SANS scattering traces for the postmixed samples are shown in Figure 4 as well as Figures S7 and S8. As shown here, for each profile at different temperatures for both micellar systems, the scattering intensity decreases monotonically with time and ultimately approaches that of the premixed solution. Note that the difference in scattering intensity between the premixed sample and the solvent primarily comes from the scattering of the PMMA corona chains, which are all hydrogenated for both h- and dmicelles. By integrating the scattering intensity over the q range of 0.007 < q < 0.03 and 0.007 < q < 0.023 (Å⁻¹) for the CS and TF micelles, respectively, R(t) can be obtained (Figure 5). Notably, R(t) is still ~0.2–0.4 at the end of the TR-SANS experiments. This is not due to possible chemical cross-linking of chains (Figure S9), as the sample processing conditions in the current work are relatively mild. Rather, this is because R(t)is almost logarithmic and its decay becomes extremely slow at longer times, beyond a reasonable experimental time scale. With time-temperature superposition, a master curve of R(t)vs t/a_T can be constructed for both micellar systems, as presented in Figure 6, where a_T is the shift factor. Note that R(t) of the CS micelles agrees very well with the previous data,²⁴ indicating the reproducibility of the measurements. As shown in Figure 6, it takes much more time for the TF micelles to reach the same value of R(t) than their CS counterparts,

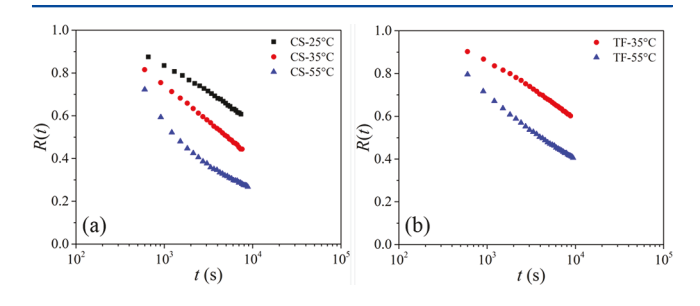


Figure 5. Relaxation function R(t) vs t at varying temperatures for the postmixed 1 wt % (a) CS and (b) TF micellar solutions in 30% [BMIM], as indicated inside the graph.

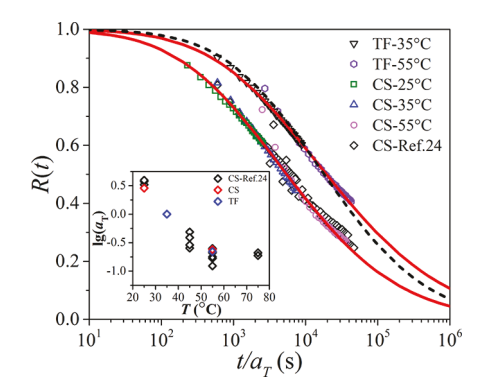


Figure 6. Time—temperature superposed R(t) vs $t/a_{\rm T}$ for 1 wt % CS and TF micelles in 30% [BMIM] ionic liquid, as indicated inside the plot. The black diamonds represent data from a previous report. ²⁴ The lines are the fits to the model described previously. ^{19,24} The red solid lines are obtained by tuning two parameters ($\alpha\chi$ and $N_{\rm w}/N_{\rm n}$) simultaneously while the black dashed line is based on one fitting parameter (f, see the text), with the $\alpha\chi$ and $N_{\rm w}/N_{\rm n}$ fixed the same as that extracted for the CS micelles. Note that the coefficient of determination $R^2=0.991$, 0.996, and 0.980, respectively, for the CS micelles, TF micelles (red line), and TF micelles (black line). The inset shows the shift factor $a_{\rm T}$ vs temperature.

indicating the chains exchange slowly in the former case. Specifically, to reach R(t)=0.5, it takes a factor of ~ 3.5 longer for the larger, TF micelles. In short, these results suggest that a micelle with a larger core size displays slower chain exchange, which must be attributed to the difference in the geometrical structure of the micelles, as the molecular characteristics of the block copolymer and the solvent are the same.

It is now commonly accepted that single chain expulsion is the rate-limiting step for unimer exchange, which is typically considered as a thermally driven first-order process, as described by Arrhenius relation

$$\tau = \tau_0 \exp\left(\frac{E_a}{k_B T}\right) \tag{2}$$

where τ is the time for chain exchange, τ_0 is the characteristic attempt time for one expulsion event, $E_{\rm a}$ is the activation energy for chain expulsion, $k_{\rm B}$ is the Boltzmann constant, and T is the absolute temperature. On this basis, Choi et al. proposed a quantitative model to successfully describe the relaxation function of the TR-SANS data in various micellar systems. The details of this model can be found in the literature. Briefly, in this model, τ_0 is assumed as the Rouse time of the core block (i.e., $\tau_0 = \tau_{\rm Rouse}$, the time for the core block to migrate to the core/corona interface), and the thermodynamic barrier for chain expulsion is represented by the product $N_{\rm core}\chi$, with a scale factor α , as given by

$$\tau = \tau_{\text{Rouse}} \exp(\alpha \chi N_{\text{core}}) \tag{3}$$

$$\tau_{\text{Rouse}} = \frac{N_{\text{core}}^2 b^2 \zeta}{6\pi^2 kT} \tag{4}$$

where $N_{\rm core}$ is the core block length and b and ζ are the statistical segment length and monomeric friction coefficient of the core block. We first fit the R(t) data of both CS and TF micelles based on Choi's model, assuming $\tau_{\rm Rouse}$ is the same between these two micelles. From this fitting, we obtained $\alpha\chi$ to be 0.012 and 0.015, respectively, for micelles prepared by the CS and TF protocols. As a result, the chain exchange time τ can

be estimated by eq 3, and from this calculation, it was found that the relaxation time in the TF micelles is retarded by a factor of 3 compared to the CS ones. Additionally, note that in this model there are two fitting parameters (assuming the Rouse time for the core block is known from a previous report 24): $\alpha \chi$, as mentioned above, and the dispersity of the core block molecular weight $(N_{\rm w}/N_{\rm n})$, which was estimated to be 1.13 for both copolymers. This value is larger than that measured by SEC (Table 1) for two reasons: first, the SEC dispersity is for the block copolymer rather than the core block; second, there is slight difference in the molecular weight of the h- and d-core blocks, which could increase the dispersity reflected in the chain exchange process.

On the other hand, in the analysis above as au_0 or au_{Rouse} is assumed to be the same between the TF and CS micelles, the observed difference in the chain exchange rates is effectively reflected in the different values of $\alpha \chi$, i.e., the activation energy. However, we note that the corona density profile is distinct between the two micelles (Figure S10). As shown there, the corona thickness is comparable between the two micelles, estimated as 2s = 12.4 and 12.2 nm, respectively, for the CS and TF micelles (s is a fitting parameter in the Pedersen model, dictating the width of the corona profile). These values are consistent with the calculations from the hydrodynamic radii (Table 2). Additionally, in both cases the corona density $\rho'(r)$ (or volume fraction) decreases monotonically with radial distance. Importantly, $\rho'(r)$ of the TF micelles is higher than that of the CS ones throughout the entire corona region (e.g., the corona chain volume fraction is ca. 0.36 and 0.52 at the core/corona interface for the CS and TF micelles, respectively). The average corona block volume fraction in the corona was estimated to be ca. 8% (or 0.6 monomers/nm³) and 11% (or 0.8 monomers/nm³), respectively, for CS and TF micelles. This could affect the diffusion time for the core block to go through the corona, which might also contribute to τ_0 , as proposed by Zinn et al.²³ Moreover, the distinct corona density between these two micelles could also affect the process of chain reinsertion. To examine this effect, we have also fit the R(t)data of the TF micelles by adjusting τ_0 while keeping the $\alpha \chi$ and $N_{\rm w}/N_{\rm n}$ the same as that extracted for the CS micelles, as

$$\tau = f\tau_{\text{Rouse}} \exp(\alpha \chi N_{\text{core}}) \tag{5}$$

where $\tau_0 = f \tau_{\text{Rouse}}$, f is the only fitting parameter, accounting for the effective contribution of the core block diffusion through the corona to τ_0 . As shown in the black dashed line in Figure 6, the fitting is slightly worse than the two-parameter model (red solid line) but is still reasonable. From this fitting, f was estimated to be ~3.05, which is consistent with the previous calculation, indicating the rate of chain exchange in the TF micelles is reduced by a factor of 3 compared to the CS ones. Overall, the relaxation function for the TF micelles can be described by either of these two models; however, this does not necessarily mean the difference in the chain exchange rates between the CS and TF micelles comes solely from the change in the activation barrier or the attempt time, as discussed below.

We first compare the diffusion time for the core block to go through the corona between these two micelles. Assume the expelled PnBMA block forms a collapsed globule in the corona $(R_{\text{collapsed}} \approx 2.7 \text{ nm} < R_{\text{g,PMMA}} \approx 4.0 \text{ nm})$; in this size regime, the concentration dependence of diffusion coefficient of the core block in the semidilute PMMA corona was reported to follow $D \sim \varphi^{-1.45}$, where φ is the PMMA volume fraction in the

corona. Thus, the diffusion time ratio for the core block to go through the corona can be estimated as $\tau_{\rm d,TF}/\tau_{\rm d,CS} = (L_{\rm corona,TF}^2/D_{\rm TF})/(L_{\rm corona,CS}^2/D_{\rm CS}) = (L_{\rm corona,TF}/L_{\rm corona,CS})^2(\varphi_{\rm CS}/\varphi_{\rm TF})^{-1.45} \approx 1.7$, where $L_{\rm corona,TF}$ and $L_{\rm corona,CS}$ are the corona thickness of the TF and CS micelles and $\varphi_{\rm CS}$ and $\varphi_{\rm TF}$ are the average PMMA volume fraction in the corona of the CS and TF micelles, respectively. Although this might partly explain the slower chain exchange kinetics for the TF micelles, it still significantly underestimates the observed difference in the rates of chain exchange, i.e., a factor of 3–3.5. This presumably indicates the activation barrier (i.e., the free energy difference before and after chain expulsion) might also be different between the two micelles.

Several factors could impact the energy barrier of the chain exchange process. First, the degree of core block stretching will be stronger for micelles with a larger core size, considering that the unperturbed core block dimension is the same (Table 2). This would contribute to lowering the entropic barrier of the chain expulsion process and thus cannot explain the finding here. On the other hand, we have to note that only a small fraction of chains has to be stretched to fill the central space of the micelle core, and hence the overall contribution of core block stretching to the chain expulsion process might be effectively negligible. Second, the degree of corona block stretching is comparable between these two micelles and thus should not bring any significant differentiation to the activation energy between these two systems (Table 2). A third difference between these two micelles is the corona density profile (Table 2 and Figure S10). As suggested by Lund et al., 27 this can effectively modify the interaction between the core block and the corona region. A denser corona in the TF micelle provides more segmental contacts between the expelled PnBMA block and the PMMA chains, leading to a smaller effective χ and thus accelerated kinetics (assuming $\chi_{PnBMA/PMMA} < \chi_{PnBMA/IL}$). This is also not consistent with the observed trend. Instead, we propose that the following two factors could lead to distinct activation barrier. First, as the interfacial area per chain (a_0) scales with R_c^{-1} , a_0 is larger for the CS micelles than that of the TF ones. Specifically, a_0 was calculated to be $16._1$ and $12._5$ nm² for micelles prepared by these two methods, respectively. As the chain has to be stretched (the cross section of a Gaussian coil $R_{g,0}^2$ for 53 kg/mol PnBMA is ~23.1 nm²) when going through the orifice of the core/corona interface, it should be entropically easier for micelles with a larger orifice or smaller core size to cross the interface, and hence a smaller chain expulsion energy barrier results. Second, Halperin calculated the work of inserting a core globule against the osmotic pressure of the corona $\Delta F_{\rm ins}/kT \sim N_{\rm agg}^{3/2}/R_{\rm c}^{3}(1+N_{\rm agg}^{-1}) \sim N_{\rm agg}^{3/2}/R_{\rm c}^{3} \sim R_{\rm c}^{3/2.28}$ Therefore, a larger core dimension leads to a denser corona (Figure S10), which then gives rise to higher insertion penalty (i.e., larger activation energy) for the core block. In summary, we speculate that it is these combined factors, affecting both the attempt time τ_0 and activation energy $E_{\rm a}$ of chain expulsion, that lead to the different chain exchange kinetics in these two micelles. However, due to the core block dispersity and the LCST behavior of the current system, the changes in τ_0 and E_a with varying micelle core sizes cannot be easily decoupled.

We next compare our finding with that of Zinn et al., ²³ who measured the chain exchange kinetics for micelles of different core sizes. Note that in this work the variation in the core dimensions results from distinct corona block lengths, with the core block length fixed. It was found that the net activation

energy corrected by heat of fusion of the core block (*n*-alkyl groups, which can crystallize within the micellar core) shows a small but systematic decrease with increasing corona block length (i.e., when the micelle core size becomes smaller). Although this result is apparently consistent with our findings, the magnitude of the changes in core size and activation energy might not exceed the experimental uncertainty. Moreover, the measured chain exchange rate actually decreased with corona block length (smaller core size), which was attributed to the slower diffusion of the expelled chains through a thicker corona region. Therefore, the comparison between these two systems must be viewed with some caution.

On the other hand, Lund et al. observed a slower rate of chain exchange (due to larger activation barrier) for cylindrical micelles compared to their spherical counterparts formed with the same polymer and solvent, which was attributed to the different conformations of the expelled core block in the corona.²⁷ This factor could be applicable to our system as well. However, it is quite unlikely that the PnBMA core block in the current system adopts a stretched conformation in the corona region, as proposed by Lund et al.,²⁷ considering the much longer contour length (~47 nm) than the corona thickness (\sim 12–14 nm). Moreover, the stretched conformation is not favorable both enthalpically and entropically. Rather, a more likely conformation for the expelled PnBMA block would be that between theta condition ($R_{\rm g,0} \approx 4.8$ nm) and a fully collapsed state ($R_{\text{collapsed}} \approx 2.7 \text{ nm}$). In such a case, the PnBMA block is presumably more expanded in the TF corona as the solvent quality is slightly better, which could impact the activation barrier of the chain expulsion process. This effect should be more dramatic near the core/corona interface, where the corona density is most distinct between these two micelles (Figure S10). Essentially, these results suggest that the curvature of the core/corona interface, dictated by the micelle core dimension, plays a critical role in the process of molecular exchange.

Going further, our data also indicate that even in a system there is appreciable chain exchange, there is no guarantee that it can easily reach equilibrium. For instance, in the current system, the chain exchange occurs on a time scale of hours, but the distinct micelle size is stable up to 2 weeks. An important question is: does either micelle size represent equilibrium under the experimental conditions, and if so, which one? In the previous work, Meli and Lodge suggested that the size upon prolonged thermal annealing from the TF protocol should be close to the thermodynamically stable value, as distinct annealing histories led to the same size. In that system, as no unimer exchange was detected, it was argued that the system relaxed from initially large and polydisperse aggregates to smaller, narrowly distributed spherical micelles through fragmentation processes. In contrast, as the initial micelle size distribution in the current system is sufficiently narrow, fusion/ fragmentation events should be energetically unfavorable and therefore the dominant mechanism for micellar relaxation is chain exchange. As the dissolution temperature (80 °C) is fairly close to the annealing temperature (55 °C), the micelles can easily reach their stable state at 55 °C. Interestingly, dissolution of the BCP chains at a higher temperature (150 °C) yields micelles with a larger size, which subsequently relax to the same size as the ones prepared at 80 °C (Figure S6). These results suggest that the TF micelles reach their equilibrated morphologies upon thermal annealing. On the other hand, our data also imply that the equilibration of the CS micelles is

still difficult or practically impossible over a reasonable time scale, even when the chain exchange is facile. We speculate that as the CS micelles typically have narrow size distributions, the system-wise equilibration should be dominated by the chain expulsion/insertion processes; yet, the relaxation from smaller micelles to larger ones via these processes requires disintegration of existing micelles, which is thermodynamically quite unfavorable. In other words, as equilibration of micelle size requires a change in the number of micelles, via either assembly/disintegration processes or fusion/fragmentation events, it is a much slower process, as in the classical Aniansson—Wall theory.⁴⁸

SUMMARY

In this report we have investigated the effect of micelle size on the chain exchange kinetics of spherical BCP micelles in imidazolium-based ionic liquids. Two micelles were prepared using two different methods, i.e., CS and TF. We have shown that both the hydrodynamic size and core dimension of the TF micelles are appreciably larger than that of the CS ones, presumably due to the different interactions between the core block and the solvent environment when micelles were formed. More interestingly, these two distinct, narrow size distributions were stable upon prolonged thermal annealing up to nearly 2 weeks. Although this suggests the practical difficulty of equilibrating this apparently simple micellar system, it provides an opportunity to exclusively examine the micellar structural effect on chain exchange, decoupled from the chain and solvent characteristics. We have found that via the TR-SANS experiments the rate of chain exchange in the TF micelles is significantly smaller than the CS ones. Two important structural differences were suggested to explain our finding, i.e., the smaller interfacial area per chain and larger average corona density in the TF micelles as a result of the larger core dimension. These factors could affect both the attempt time and activation barrier during the chain exchange process, collectively retarding the kinetics of chain exchange. These results underscore that besides the molecular characteristics of the block copolymer and the solvent, the micellar geometrical structure, which depends on the sample processing history, can also play a critical role in the molecular exchange processes in block copolymer micelles.

ASSOCIATED CONTENT

S Supporting Information

The Supporting Information is available free of charge on the ACS Publications website at DOI: 10.1021/acs.macromol.7b02550.

¹H NMR spectra of the ionic liquids, composition of the ionic liquids in the contrast-matching solvent mixture, structural information for the *d*-micelles, additional fitting parameters from the Pedersen model, NMR characterization of the BCP dissolution, SANS traces of the protonated micelles, additional SAXS data for TF micelles, effect of solvent composition on hydrodynamic and core size distributions of CS micelles, prolonged thermal annealing light scattering experiments, additional representative TR-SANS profiles, examination of core block chemical cross-linking, corona density profiles (Figures S1–S10, Tables S1–S3) (PDF)

AUTHOR INFORMATION

Corresponding Author

*E-mail: lodge@umn.edu (T.P.L.).

ORCID

Timothy P. Lodge: 0000-0001-5916-8834

Notes

The authors declare no competing financial interest.

ACKNOWLEDGMENTS

The authors acknowledge financial support from National Science Foundation (DMR-1707578). Portions of this work were performed at the DuPont-Northwestern-Dow Collaborative Access Team (DND-CAT) located at Sector 5 of the Advanced Photon Source (APS). DND-CAT is supported by Northwestern University, E.I. DuPont de Nemours & Co., and The Dow Chemical Company. This research used resources of the Advanced Photon Source, a U.S. Department of Energy (DOE) Office of Science User Facility operated for the DOE Office of Science by Argonne National Laboratory under Contract DE-AC02-06CH11357. We acknowledge the support of the National Institute of Standards and Technology (NIST), U.S. Department of Commerce, in providing the neutron research facilities used in this work. We thank Dr. Yimin Mao and Dr. Paul Butler for their assistance in SANS measurements. The NIST Center for Neutron Research is also acknowledged for providing access to the DynaPro NanoStar instrument. We thank Frank Bates, En Wang, and David Morse for helpful discussions.

■ REFERENCES

- (1) Kataoka, K.; Harada, A.; Nagasaki, Y. Block copolymer micelles for drug delivery: design, characterization and biological significance. *Adv. Drug Delivery Rev.* **2001**, *47*, 113–131.
- (2) Tyrrell, Z. L.; Shen, Y.; Radosz, M. Fabrication of micellar nanoparticles for drug delivery through the self-assembly of block copolymers. *Prog. Polym. Sci.* **2010**, 35, 1128–1143.
- (3) Park, T. G.; Jeong, J. H.; Kim, S. W. Current status of polymeric gene delivery systems. *Adv. Drug Delivery Rev.* **2006**, 58, 467–486.
- (4) Lee, R. C.; River, L. P.; Pan, F.-S.; Ji, L.; Wollmann, R. L. Surfactant-induced sealing of electropermeabilized skeletal muscle membranes in vivo. *Proc. Natl. Acad. Sci. U. S. A.* **1992**, *89*, 4524–4528.
- (5) Hartgerink, J. D.; Beniash, E.; Stupp, S. I. Self-assembly and mineralization of peptide-amphiphile nanofibers. *Science* **2001**, *294*, 1684–1688.
- (6) Anderson, W. Block Copolymers as Viscosity Index Improvers for Lubrication Oils. U.S. Patent 3763044, 1973.
- (7) Vriezema, D. M.; Comellas Aragonès, M.; Elemans, J. A.; Cornelissen, J. J.; Rowan, A. E.; Nolte, R. J. Self-assembled nanoreactors. *Chem. Rev.* **2005**, *105*, 1445–1490.
- (8) Könczöl, L.; Döll, W.; Buchholz, U.; Mülhaupt, R. Ultimate properties of epoxy resins modified with a polysiloxane—polycaprolactone block copolymer. *J. Appl. Polym. Sci.* **1994**, *54*, 815–826.
- (9) Dean, J.; Lipic, P.; Grubbs, R.; Cook, R.; Bates, F. Micellar structure and mechanical properties of block copolymer-modified epoxies. *J. Polym. Sci., Part B: Polym. Phys.* **2001**, 39, 2996–3010.
- (10) Ruzette, A.-V.; Leibler, L. Block copolymers in tomorrow's plastics. *Nat. Mater.* **2005**, *4*, 19–31.
- (11) Nicolai, T.; Colombani, O.; Chassenieux, C. Dynamic polymeric micelles versus frozen nanoparticles formed by block copolymers. *Soft Matter* **2010**, *6*, 3111–3118.
- (12) Honda, C.; Hasegawa, Y.; Hirunuma, R.; Nose, T. Micellization kinetics of block copolymers in selective solvent. *Macromolecules* **1994**, 27, 7660–7668.

(13) Tian, M.; Qin, A.; Ramireddy, C.; Webber, S. E.; Munk, P.; Tuzar, Z.; Prochazka, K. Hybridization of block copolymer micelles. *Langmuir* 1993, 9, 1741–1748.

- (14) Wang, Y.; Kausch, C. M.; Chun, M.; Quirk, R. P.; Mattice, W. L. Exchange of chains between micelles of labeled polystyrene-block-poly(oxyethylene) as monitored by nonradiative singlet energy transfer. *Macromolecules* 1995, 28, 904–911.
- (15) Schaeffel, D.; Kreyes, A.; Zhao, Y.; Landfester, K.; Butt, H.-J.; Crespy, D.; Koynov, K. Molecular Exchange Kinetics of Diblock Copolymer Micelles Monitored by Fluorescence Correlation Spectroscopy. ACS Macro Lett. 2014, 3, 428–432.
- (16) Esselink, F.; Dormidontova, E.; Hadziioannou, G. Evolution of block copolymer micellar size and structure evidenced with cryo electron microscopy. *Macromolecules* **1998**, *31*, 2925–2932.
- (17) Esselink, F.; Dormidontova, E.; Hadziioannou, G. Redistribution of block copolymer chains between mixed micelles in solution. *Macromolecules* **1998**, *31*, 4873–4878.
- (18) Willner, L.; Poppe, A.; Allgaier, J.; Monkenbusch, M.; Richter, D. Time-resolved SANS for the determination of unimer exchange kinetics in block copolymer micelles. *Europhys. Lett.* **2001**, *55*, 667–673.
- (19) Choi, S.-H.; Lodge, T. P.; Bates, F. S. Mechanism of molecular exchange in diblock copolymer micelles: hypersensitivity to core chain length. *Phys. Rev. Lett.* **2010**, *104*, 047802.
- (20) Lu, J.; Choi, S.; Bates, F.; Lodge, T. Molecular exchange in diblock copolymer micelles: bimodal distribution in core-block molecular weights. *ACS Macro Lett.* **2012**, *1*, 982–985.
- (21) Lund, R.; Willner, L.; Richter, D.; Dormidontova, E. E. Equilibrium chain exchange kinetics of diblock copolymer micelles: Tuning and logarithmic relaxation. *Macromolecules* **2006**, *39*, 4566–4575.
- (22) Lund, R.; Willner, L.; Stellbrink, J.; Lindner, P.; Richter, D. Logarithmic chain-exchange kinetics of diblock copolymer micelles. *Phys. Rev. Lett.* **2006**, *96*, 068302.
- (23) Zinn, T.; Willner, L.; Pipich, V.; Richter, D.; Lund, R. Molecular exchange kinetics of micelles: corona chain length dependence. *ACS Macro Lett.* **2016**, *5*, 884–888.
- (24) Ma, Y.; Lodge, T. P. Chain Exchange Kinetics in Diblock Copolymer Micelles in Ionic Liquids: The Role of χ . *Macromolecules* **2016**, 49, 9542–9552.
- (25) Lu, J.; Bates, F. S.; Lodge, T. P. Remarkable Effect of Molecular Architecture on Chain Exchange in Triblock Copolymer Micelles. *Macromolecules* **2015**, *48*, 2667–2676.
- (26) Halperin, A.; Alexander, S. Polymeric micelles: their relaxation kinetics. *Macromolecules* **1989**, *22*, 2403–2412.
- (27) Lund, R.; Willner, L.; Pipich, V.; Grillo, I.; Lindner, P.; Colmenero, J.; Richter, D. Equilibrium chain exchange kinetics of diblock copolymer micelles: Effect of morphology. *Macromolecules* **2011**, *44*, 6145–6154.
- (28) Halperin, A. On Micellar Exchange: The Role of the Insertion Penalty. *Macromolecules* **2011**, *44*, 5072–5074.
- (29) Choi, S.-H.; Bates, F. S.; Lodge, T. P. Molecular exchange in ordered diblock copolymer micelles. *Macromolecules* **2011**, *44*, 3594–3604.
- (30) Zhang, L.; Eisenberg, A. Thermodynamic vs kinetic aspects in the formation and morphological transitions of crew-cut aggregates produced by self-assembly of polystyrene-b-poly (acrylic acid) block copolymers in dilute solution. *Macromolecules* **1999**, 32, 2239–2249.
- (31) Desbaumes, L.; Eisenberg, A. Single-solvent preparation of crew-cut aggregates of various morphologies from an amphiphilic diblock copolymer. *Langmuir* 1999, 15, 36—38.
- (32) Cameron, N. S.; Corbierre, M. K.; Eisenberg, A. 1998 EWR Steacie Award Lecture Asymmetric amphiphilic block copolymers in solution: a morphological wonderland. *Can. J. Chem.* 1999, 77, 1311–1326.
- (33) Meli, L.; Lodge, T. P. Equilibrium vs metastability: High-temperature annealing of spherical block copolymer micelles in an ionic liquid. *Macromolecules* **2009**, *42*, 580–583.

(34) Meli, L.; Santiago, J. M.; Lodge, T. P. Path-dependent morphology and relaxation kinetics of highly amphiphilic diblock copolymer micelles in ionic liquids. *Macromolecules* **2010**, *43*, 2018–2027.

- (35) Lee, H.-N.; Lodge, T. P. Poly(*n*-butyl methacrylate) in ionic liquids with tunable lower critical solution temperatures (LCST). *J. Phys. Chem. B* **2011**, *115*, 1971–1977.
- (36) Ma, Y.; Lodge, T. P. Poly(methyl methacrylate)-block-poly(n-butyl methacrylate) Diblock Copolymer Micelles in an Ionic Liquid: Scaling of Core and Corona Size with Core Block Length. *Macromolecules* **2016**, *49*, 3639–3646.
- (37) Hoarfrost, M. L.; He, Y.; Lodge, T. P. Lower Critical Solution Temperature Phase Behavior of Poly(*n*-butyl methacrylate) in Ionic Liquid Mixtures. *Macromolecules* **2013**, *46*, 9464–9472.
- (38) Bonhote, P.; Dias, A.-P.; Papageorgiou, N.; Kalyanasundaram, K.; Grätzel, M. Hydrophobic, highly conductive ambient-temperature molten salts. *Inorg. Chem.* **1996**, *35*, 1168–1178.
- (39) Dzyuba, S. V.; Li, S.; Bartsch, R. A. Convenient syntheses of perdeuterated ionic liquids. *J. Heterocycl. Chem.* **200**7, 44, 223–225.
- (40) Wiley, R. H.; Brauer, G. Refractometric determination of second-order transition temperatures in polymers. II. Some acrylic, vinyl halide, and styrene polymers. *J. Polym. Sci.* 1948, *3*, 455–461.
- (41) Frisken, B. J. Revisiting the method of cumulants for the analysis of dynamic light-scattering data. *Appl. Opt.* **2001**, *40*, 4087–4091.
- (42) Jakeš, J. Regularized positive exponential sum (REPES) program A way of inverting laplace transform data obtained by dynamic light scattering. *Collect. Czech. Chem. Commun.* **1995**, *60*, 1781–1797.
- (43) Pedersen, J. S.; Svaneborg, C.; Almdal, K.; Hamley, I. W.; Young, R. N. A small-angle neutron and X-ray contrast variation scattering study of the structure of block copolymer micelles: Corona shape and excluded volume interactions. *Macromolecules* **2003**, *36*, 416–433.
- (44) Pedersen, J. S. Determination of size distribution from small-angle scattering data for systems with effective hard-sphere interactions. *J. Appl. Crystallogr.* **1994**, *27*, 595–608.
- (45) Glinka, C.; Barker, J.; Hammouda, B.; Krueger, S.; Moyer, J.; Orts, W. The 30 m small-angle neutron scattering instruments at the National Institute of Standards and Technology. *J. Appl. Crystallogr.* **1998**, *31*, 430–445.
- (46) Kline, S. R. Reduction and analysis of SANS and USANS data using IGOR Pro. *J. Appl. Crystallogr.* **2006**, *39*, 895–900.
- (47) Kohli, I.; Mukhopadhyay, A. Diffusion of nanoparticles in semidilute polymer solutions: effect of different length scales. *Macromolecules* **2012**, *45*, 6143–6149.
- (48) Aniansson, E.; Wall, S.; Almgren, M.; Hoffmann, H.; Kielmann, I.; Ulbricht, W.; Zana, R.; Lang, J.; Tondre, C. Theory of the kinetics of micellar equilibria and quantitative interpretation of chemical relaxation studies of micellar solutions of ionic surfactants. *J. Phys. Chem.* **1976**, *80*, 905–922.